Chapter 46

Diffusion media materials and characterisation

Mark Mathias[1], Joerg Roth[2], Jerry Fleming[3] and Werner Lehnert[4]

[1] *General Motors – Global Alternative Propulsion Center, Honeoye Falls, NY, USA*
[2] *Adam Opel AG – Global Alternative Propulsion Center, Rüsselsheim, Germany*
[3] *Spectracorp, Inc., Lawrence, MA, USA*
[4] *Center for Solar Energy and Hydrogen Research Baden-Württemberg, Ulm, Germany*

1 INTRODUCTION

Polymer electrolyte fuel cell (PEFC) stacks usually employ bipolar plates with channels on either side for the distribution of reactants over the electrode surfaces. Figure 1 shows the cross-section of a small section from such a PEFC. At the center of the structure is a 50 μm membrane coated by two 15 μm catalyst layers on either side. Surrounding this, two roughly 200 μm thick carbon-fiber paper gas-diffusion media are clearly observed. These are adjacent to two bipolar plate sections, the anode plate on the top and the cathode plate on the bottom. The coolant channels are adjacent to the air channels in the cathode plate. The region between reactant channels consists of lands, also known as ribs. In this design, roughly half of the electrode area is adjacent to channels and half is adjacent to lands. The role of the gas-diffusion media is to transition with minimum voltage loss, from the channel-land structure of the flow field to the active area of the electrode. Although all of the current passes through these lands, effective diffusion media will promote a uniform current distribution at the adjacent catalyst layer.

We refer again to Figure 1 and observe that the gas-diffusion media has several specific functions:

- Reactant permeability: provide reactant gas access from flow-field channels to catalyst layers including in-plane permeability to regions adjacent to lands;
- Product permeability: provide passage for removal of product water from catalyst-layer area to flow-field channels including in-plane permeability from regions adjacent to lands;
- Electronic conductivity: provide electronic conductivity from bipolar plates to catalyst layers including in-plane conductivity to regions adjacent to channels.
- Heat conductivity: provide for efficient heat removal from membrane electrode assembly (MEA) to bipolar plates where coolant channels are located; and
- Mechanical strength: provide mechanical support to the MEA in case of reactant pressure difference between the anode and cathode gas channels, maintain good contact (i.e., good electrical and thermal conductivity) with the catalyst layer, and not to compress into channels resulting in blocked flow and high channel pressure drops.

The above functions impose requirements on diffusion media physical and mechanical properties. The in-plane conductivity and permeability requirements are more demanding as compared with the through-plane (i.e., perpendicular to the membrane) requirements due to the aspect ratio of the land-width and channel-width relative to the diffusion media thickness. This is discussed in more detail below in the context of electrical conductivity requirements.

In addition to optimizing bulk properties which can depend significantly on compression, the interfacial electrical and thermal conductivities with the bipolar plate and

---

Handbook of Fuel Cells – Fundamentals, Technology and Applications, Edited by Wolf Vielstich, Hubert A. Gasteiger, Arnold Lamm.
Volume 3: *Fuel Cell Technology and Applications*.

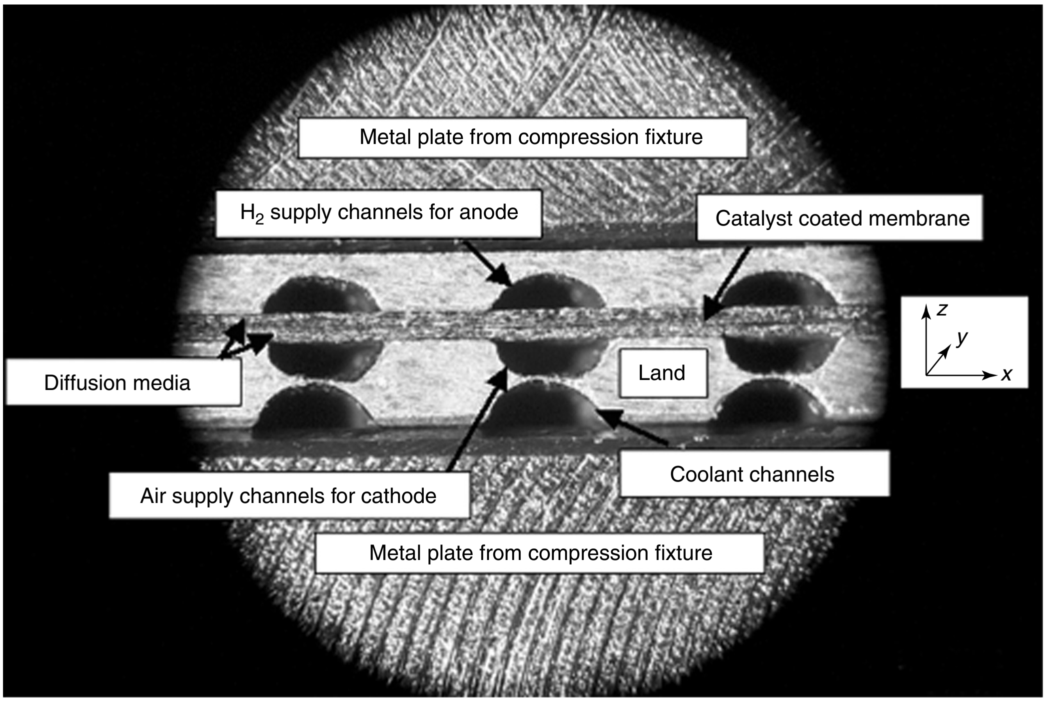

Figure 1. Cross-sectional view of a small section from a PEFC. A catalyst-coated membrane is sandwiched between two gas-diffusion media (Toray TGP−H−060), which are in turn held between two plate sections containing flow channels. The width of the land is approximately 1.5 mm.

the catalyst layers must be optimized. These interfacial conductivities are typically strong functions of compression. Thus, the diffusion media, the neighboring materials, and the stack compression must be optimized together.

The basic nature of the flow-field design also dictates diffusion media requirements. In the case of interdigitated designs,[1] the diffusion media convective permeability must be high enough to permit gas passage without excessive pressure drop. Even with more conventional serpentine designs,[2] convection through the diffusion media due to adjacent channel pressure drop must be optimized. We note that there are PEFC design concepts in which flow channels are not used to distribute flow, such as those using meshes;[3, 4] such designs substantially change the diffusion media requirements. We will restrict the scope of this chapter to diffusion media for use with conventional channel-based flow fields.

Because of the variety of ways of constructing a PEFC (see **Principles of MEA preparation**, Volume 3), there is potential for confusion when referring to the subcomponents. When catalyst-coated membranes are employed, diffusion media are positioned adjacent to and bonded or pressed against the catalyst layers. In another configuration, a catalyst layer is coated on the diffusion media which functions as a support, and two of these catalyst-coated substrates are hot-pressed on either side of a membrane to make a five-layer assembly. In this case, the catalyst-coated substrate can be referred to as a gas-diffusion electrode, because the electrocatalysis and gas-diffusion functions have been intimately mixed into a single component. The term gas-diffusion electrode has also been used to refer to PEFC catalyst layers themselves,[5] since they must allow efficient gas diffusion to achieve good catalyst utilization. In this chapter however, we will restrict our attention to the region where no electrochemical reaction occurs, adjacent to the catalyst layer. Therefore, we use the term gas-diffusion media and not gas-diffusion electrode.

The term gas-diffusion electrode, although sometimes used to discuss PEFC components, is even more common in the phosphoric acid fuel cell (PAFC) literature. This is because the best performing PAFC fuel cells involve supporting the catalyst on carbon-fiber paper that is made hydrophobic in order to retain the liquid electrolyte between the two electrodes. Note that the PEFC diffusion media has a quite different requirement, that of wicking liquid water produced at the cathode away to the gas channels. Nevertheless, a large body of work seeking to understand and optimize these structures for PAFC application is available (see **Catalyst studies and coating technologies**, Volume 3),[6] and many of the issues (e.g., polytetrafluoroethylene (PTFE) distribution) and characterization techniques (e.g., pore size distribution, wetting properties) that are prominent in that literature are common to PEFC diffusion media. Thus the PAFC work provides interesting historical context to PEFC gas-diffusion-media development.

The current strong interest in PEFC development is leading to a steadily growing body of patents relevant to PEFC gas-diffusion-media design, optimization, and production, and we next reference a small subset of these patents. Patents exist disclosing production and/or use of a wide variety of substrates, for example: carbon-fiber paper,[7] coated or filled carbon cloths,[8, 9] and carbon-filled nonwoven webs.[10] Tailoring the gas permeability[11] and ratio of hydrophobic/hydrophilic pores[12] have been proposed in order to optimize performance. Methods to tailor the properties of electronically conductive substrates, such as carbon cloths, by filling or coating with bound carbon particles have been proposed for use in PEFCs.[13, 14] Concepts exist for integrating flow channels into the diffusion-media,[15] and for sewing hydrophilic threads through the diffusion-media backing in order to more effectively transport liquid water within the cell.[16]

There is very little published scientific work on PEFC gas-diffusion media, and what is available is of an applied nature. For example, Ballard and Johnson Matthey have shown that cloth and paper diffusion media can result in very different polarization behavior in the high current density ($>0.5\,\mathrm{A\,cm^{-2}}$) range.[17] The role of PTFE-bound carbon-powder gas-diffusion layers positioned between the catalyst layer and the gas-diffusion media has been examined, both for carbon-fiber paper[18] and carbon cloth[19] substrates. In both cases, the composition and carbon type within these layers are shown to influence the onset of flooding at high current densities. Lee *et al.* studied the interactions between gas-diffusion-media type, gasket thickness, and compression, showing that these variables must be optimized together in order to obtain optimum performance.[20]

The lack of published work perhaps reflects the fact that current diffusion media is typically not a major source of voltage loss within state-of-the-art PEFCs (**Beginning-of-life MEA performance — Efficiency loss contributions**, Volume 3). However, this component will receive additional attention as focus shifts from steady-state performance to cold-start and stability, issues that will require tailoring of the diffusion media to more efficiently deal with liquid water under a variety of conditions. Durability concerns also increase focus on the diffusion media, particularly since mechanical creep of the membrane due to pressure from the adjacent diffusion media must be understood and minimized. Finally, cost considerations dictate improvements in diffusion-media design and processing; current pricing for this component is in the neighborhood of $50 per kW against an automotive target of less that $5 per kW. Clearly, significant PEFC diffusion-media development effort is still critically needed.

2 CARBON-FIBER-BASED DIFFUSION MEDIA

The most promising candidates for use as diffusion media in PEFCs are carbon-fiber-based products, such as nonwoven papers and woven fabrics (or cloths), due to their high porosity (≥70%) and good electrical conductivity. They have been commercialized in other applications and are now being adapted to PEFCs. Graphitized-carbon-fiber paper is used to make gas-diffusion electrodes for phosphoric acid fuel cells. Carbon cloth is used in friction and wear applications, such as in automotive transmissions and aircraft brakes. Typical properties of these two materials are

Table 1. Typical properties of carbon-fiber paper and carbon fiber cloth.

	Method	Carbon-fiber paper[a]	Woven fabric[b]
Thickness (mm)	Calipers at 7 kPa	0.19	0.38
Areal weight ($\mathrm{g\,m^{-2}}$)	Gravimetric	85	118
Density ($\mathrm{g\,cm^{-3}}$)	At 7 kPa calculated	0.45	0.31
Resistance (through-plane, $\Omega\,\mathrm{cm}^2$)	Two flat graphite blocks at 1.3 MPa	0.009[c]	0.005[c]
Bulk resistivity (through-plane, Ω cm)	Mercury contacts	0.08	Not available
Bulk resistivity (in-plane, Ω cm)	Four point probe	0.0055[d]	0.009[d]
Gas permeability (through-plane, Darcys)	Gurley 4301 permeometer	8[e]	55[e]
Material description		Toray TGP–H–060	Avcarb 1071 HCB

[a] Reported by Toray (unless indicated otherwise).
[b] Reported by Ballard Material Systems (unless indicated otherwise).
[c] Measured at General Motors (GM), includes diffusion-media bulk resistance and two contact resistances (plate to diffusion media).
[d] Measured at GM, uncompressed, average of resistivity in machine and cross-machine direction.
[e] Measured at GM, uncompressed, see equation (12), 1 Darcy $= 10^{-12}\,\mathrm{m}^2$.

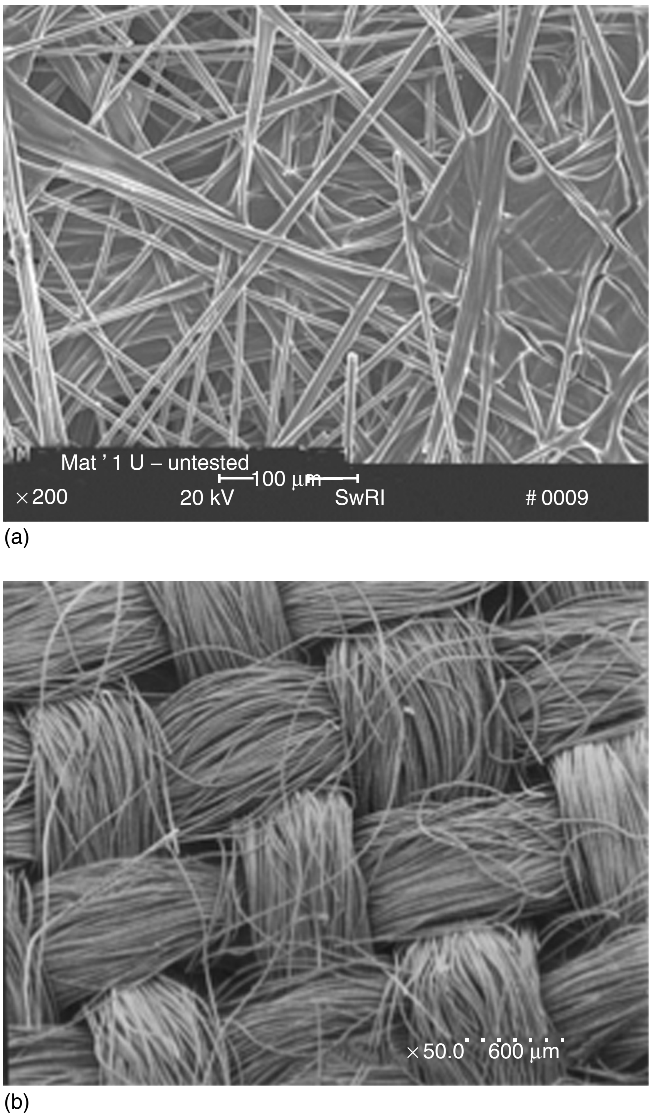

Figure 2. Micrographs (scanning electron microscope (SEM)) of two gas-diffusion-media substrates, both with approximately 7 µm diameter fibers. (a) Carbon fiber paper, Spectracorp 2050A, with no PTFE. Reference bar indicates 100 µm. (b) Carbon cloth, Textron Avcarb 1071 HCB. Reference bar indicates 600 µm.

shown in Table 1, and micrographs of each are shown in Figure 2. The micrographs show that the carbon-fiber paper is bound by webbing (carbonized thermoset resin), whereas no binder is needed in the carbon cloth due to its woven structure. Below we describe the materials and processes used to make these and other candidate carbon-fiber-based diffusion media.

2.1 Carbon fibers

Carbon fibers were first commercialized in the 1950s and are useful in a variety of markets due to their high stiffness, high strength, and light weight. The most popular choice as a starting fiber for the production of carbon-fiber-based diffusion media is a copolymer comprising greater than 90% polyacrylonitrile (PAN). Carbon fibers can also be made from heavy fractions of petroleum or coal; these are called pitch-precursed-carbon fibers, and they have been produced for many years. Carbon fibers produced from low cost versions of this material (isotropic pitch) have relatively poor structural, electrical, and thermal properties relative to PAN-based fibers. Carbon fibers can be produced from an upgraded and more costly material, called mesophase pitch; these have properties competitive with PAN-precursed material. Other carbon-fiber sources have included cellulose (e.g., Rayon) and phenolic (e.g., Kynol®) starting materials.

PAN-precursed-carbon fiber remains the most attractive material due to precursor cost, high carbon yield (50%), and carbon-fiber properties; we will focus our discussion on processing routes using this starting material. The PAN-fiber market was 2 400 000 metric tons in 2000, mostly for use in the huge acrylic textile market. The worldwide carbon-fiber market was only 15 000 metric tons in 2000, greater than 90% of which was supplied by PAN-precursed-carbon fibers. Thus, the demand for PAN fibers to produce carbon fiber taps into a vast supply and currently consumes less than 1% of the worldwide PAN-fiber market.[21]

2.2 Carbon-fiber products and processing routes

Figure 3 shows processing routes that can be used to make PAN-fiber-based diffusion media that have been proposed for PEFC use. Below we describe the processing routes associated with each of the material choices. Three of the four routes use continuous roll-good processing, desirable from a cost and manufacturability point of view. The last two steps in carbon-fiber-paper production are batch processes. Common to all routes are the steps of fiber formation and stabilization.

2.2.1 PAN-fiber formation and stabilization

PAN fibers are usually made from the PAN polymer using a solvent spinning process. The continuous fiber from this process that is used for diffusion-media production comprises large tow (320 000 filaments) with individual filament diameter of 12–14 µm. Prior to carbonization, this continuous fiber is stabilized in air at approximately 230 °C; this transforms the fiber from a thermoplastic to a thermoset material so that on subsequent heating the material does not melt but retains its form as isolated filaments.

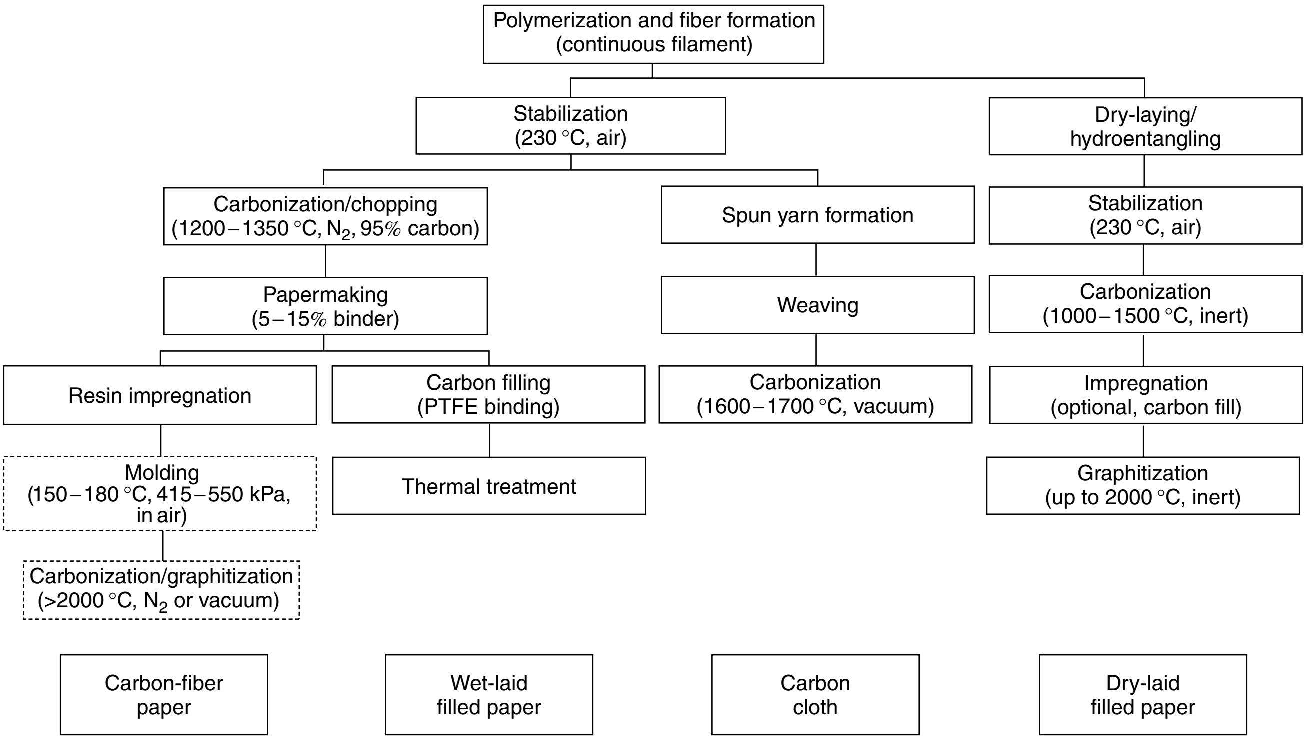

Figure 3. Various processing routes for producing PEFC diffusion-media materials using PAN-based carbon fibers. Carbon-fiber paper and carbon cloth are currently available commercial products whereas the filled materials are just now emerging as diffusion-media candidates. Two steps in carbon-fiber-paper production with dotted borders are currently batch processes; others are continuous.

2.2.2 Carbon-fiber-paper production

The non-woven substrates most often used as gas-diffusion media in fuel cells are wet-laid carbon-fiber papers which subsequently undergo further manufacturing steps in order to improve physical, electrical, and chemical properties. These materials are produced as indicated by the leftmost production path shown in Figure 3. Although the finished product is often referred to as carbon-fiber paper, this material is best described as a carbon-carbon composite since after heat treatment it consists of carbon fibers held together by a carbon matrix, as described below. The term “carbon-fiber paper” is probably better applied to the intermediate material obtained from the paper-making process. However, in this chapter we keep to current practice and will refer to the finished product as carbon-fiber paper. Current manufacturers of this material are Toray (Japan) and Spectracorp (US, Figure 2(a)).

Fiber carbonization

Stabilized-carbon fibers are heated to approximately 1200–1350 °C in nitrogen, losing 50% of their weight in the process due to loss of elemental nitrogen, oxygen, and hydrogen. Carbonization yields a fiber with >95% carbon content and physical properties of >2800 MPa tensile strength, >220 000 MPa tensile modulus, densities from 1.75–1.90 g cm^{-3}, and fiber diameter of approximately 7 μm. Although the terms ‘carbonized’ and ‘graphitized’ have at times been used interchangeably, the majority of fibers used in diffusion media have in fact only been taken to carbonization temperatures (<2000 °C) prior to paper formation; they are graphitized in the last processing step. For use in carbon-fiber paper, the tows are then chopped into 3–12 mm lengths in preparation for papermaking. Beginning with the chopped carbon fiber, the manufacture of a non-woven carbon fiber paper is a four-step process consisting of papermaking, impregnation, molding, and heat treatment (carbonization/graphitization).

Papermaking

Continuous rolls of carbon-fiber paper are manufactured using a wet-laid process using conventional papermaking equipment. During this process, the chopped carbon fiber is dispersed in water with binders, typically polyvinyl alcohol. This dispersion, which may be as low as 0.01% by weight of the fiber, is fed to a ‘headbox’ which drops the dispersion onto a rotating porous drum or wire screen with a vacuum dryer to remove the water. The still-wet web is pulled off of the far side of the drum or screen and fully dried in an oven or on hot, large diameter (1–2 m) rotating drums. The material is then continuously rolled up at the end of the drying procedure. Typical roll lengths are 250 m, with widths of up to 2 m possible. Binder content after papermaking is typically 5–15% by weight. These materials exhibit a preponderance of fibers laid out in the machine direction due to the manufacturing process, in which fibers are drawn in the machine direction as they are deposited into the fiber mat. Even with agitation in the headbox, the machine to cross-machine orientation as indicated by in-plane resistance measurements is generally 1.5 : 1, and this can approach 4 or 5 : 1 with no headbox agitation. Typical areal weights for papers at this stage of processing (prior to resin addition) are 45–70 $g\,m^{-2}$; these weights result in final carbon-fiber-paper thickness of 0.20–0.27 mm.

Resin impregnation

The rolls of carbon-fiber paper are subsequently continuously impregnated with a carbonizable thermoset resin that allows the paper to be subsequently molded to a desired thickness and density. Phenolic resins are typically used due to their carbon yield (50% of initial weight) and low cost. After impregnation with the phenolic resin, usually from a methanol-based solvent, the material is heated to approximately 150 °C in air for solvent evaporation and resin oligomerization (called B-staging). The degree of polymerization is sufficient so that there is very little resin flow during the subsequent molding step. Typical resin retention from the methanol-based solvent ranges from 50 to 70% by weight on the dried impregnated material. After impregnation, the material is usually die cut into discrete sheets of up to approximately 1 × 1 m for subsequent batch processing.

Molding

The impregnated carbon-fiber paper is compression molded and fully cured by heating to 175 °C under a pressure of 400–550 kPa. This is currently a batch process; papers are stacked up with silicone-coated separator papers between each. The stack can be molded at a given pressure or more commonly to a given thickness (called "molding to stops") to achieve the desired thickness and density. Although the resin system cures quickly at molding temperatures, large stacks need to be kept at temperature for several hours to conduct heat to the center of the stack.

If a thicker material is desired, multiple plies can be bonded together by leaving out the separator papers to achieve increased thickness while maintaining density and other physical properties. Care has to be taken in multi-ply molding to ensure that each ply is oriented in the same direction, as otherwise the differential shrinkage due to the machine-to-crossmachine ratio can result in warped parts. Following molding, a post-cure is performed at 200 °C in air for several hours to ensure full curing or crosslinking (called C-staging) of the binder material before carbonization.

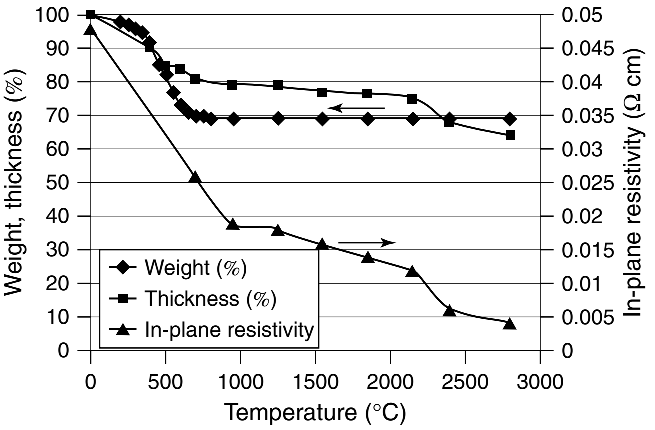

Figure 4. Carbon-fiber/phenolic-molded composite weight, thickness, and in-plane resistivity as a function of final heat treatment temperature. During graphitization (beginning at 2000 °C) the thickness and resistivity decrease, but there is no change in weight.

Carbonization/graphitization

Figure 4 shows the effect of inert-gas heat-treatment temperature on weight, thickness, and resistivity for a carbon-fiber/phenolic non-woven that has been molded and cured. Note that during heat treatment the composite material loses approximately 30–40% of its initial weight and thickness, depending upon final heat treatment temperature. Most of the property change occurring at less than 1000 °C is due to decomposition of the phenolic resin, as the carbon fiber has already been heat treated to approximately 1300 °C prior to papermaking. There is a dramatic decrease in thickness and resistivity in the 2200–2400 °C range, with no corresponding weight loss, due to the fiber transition from carbon to graphite.

The fiber graphitization at over 2000 °C changes the fiber physical structure from amorphous carbon to crystalline lamellar graphite, resulting in higher tensile modulus, increased electrical and thermal conductivity, and higher density and chemical (oxidative) resistance relative to amorphous carbon fiber. The lamellar planes of the graphitized fibers run parallel to the fiber axis, resulting in electrical and strength properties that are over an order of magnitude more favorable in the axial vs. the radial direction. Graphitization yields a fiber with >99% carbon content and physical properties of >1400 MPa tensile strength, >310 000 MPa tensile modulus, densities ranging from 1.9–2.0 $g\,cm^{-3}$, and fiber diameter of approximately 6.5 μm. In contrast to the fiber, the resin-based portion of the composite does not graphitize in this treatment but remains as amorphous carbon. This portion of the composite attains a density of approximately 1.65 $g\,cm^{-3}$ in the final product.

Carbonization and graphitization are typically achieved by stacking many sheets in a horizontal or vertical batch furnace. All heat-treating is done in an inert gas environment (nitrogen or argon), sometimes under vacuum. Some furnaces are equipped with graphite pushers which enter the top of the furnace through high temperature seals. These pushers are set to maintain a constant pressure on the stack. It is preferable to carbonize (temperatures >1200 °C) and graphitize (temperatures >2000 °C) the material in the same furnace in a continuous cycle to avoid the delays and expense of cooling and reheating the stack. Typical carbonizing cycles have slow ramp rates and holds at various temperatures to allow time for the gas to escape. After reaching 1000 °C, the material can subsequently be brought fairly rapidly to the desired final temperature. The corrosive environment of phosphoric acid cells requires nearly complete graphitization, demanding heat treatment to 2700 °C or higher, whereas the required final temperature for the PEFC application is not yet clear. The finished products are available in sizes in excess of one meter square and in thickness ranging from 0.15 to 0.30 mm.

2.2.3 Wet-laid filled papers

Figure 3 shows another approach to producing what might be called a "wet-laid filled paper" diffusion media for use in PEFCs. In this approach, a carbon or graphite powder is added to the wet-laid carbon paper and bound (e.g., with PTFE). One relies on the powder to provide conductivity rather than relying on a final carbonization or graphitization step to deliver the needed properties. This approach offers the advantage that the binder can also impart hydrophobic properties to the material. Companies currently developing products using this approach are Lydall (US) and Technical Fibre Products (UK) in cooperation with Johnson Matthey (UK). An example of a product made this way is shown in Figure 5(a) in which one observes the carbon-fiber skeleton filled with carbon powder.

2.2.4 Carbon-fiber-cloth production

The carbon fabrics used as gas-diffusion media are woven from spun PAN yarns and are subsequently carbonized or graphitized using continuous, batch or a combination of both processes. Rather than being held together by resin, their woven structure provides the mechanical integrity needed. The processing sequence is shown by the third column in Figure 3.

Yarn production

Using a stabilized large count acrylic tow (160 000 or 320 000 filaments) as the precursor, a spun yarn is produced. Typically the Worsted process is employed although other processes may be used. The Worsted process consists of running the precursor through a stretch-breaking machine, which pulls the tow between nip rolls at faster rate than it releases it. The result is a randomized breaking of all the filaments which keeps the tow in a continuous form but with fiber lengths of 1.3–5 cm long. Stabilized tow is used because of its approximately 15% strain to failure, which allows the randomized breaking. The material is then run through equipment that blends and homogenizes the material while increasing the effective yield (in length per kilogram) of the yarn. Next is a spinning operation wherein a certain number of twists or turns per length are imparted to the yarn to hold it together. The yarn is then plied (two-ply is normal) and wound on a bobbin for use in weaving or other textile operations.

Weaving

There are a wide variety of constructions that can be used in weaving a fabric. The two most popular are plain weave and eight harness satin. In a plain weave, the fill yarn (cross-machine direction) goes up and over every warp yarn (machine direction), creating a very tight fabric. In an eight harness satin weave, the fill yarn goes over seven warp yarns before going under one warp yarn and then repeating. This produces a looser, more drapable material that is typically used in structural fabrics. Plain weave is usually the construction employed in gas-diffusion media because of its dimensional stability. The woven rolls of continuous fabric require carbonization usually to a minimum of 1600 °C, sometimes done under vacuum. Producers of carbon cloth are Ballard Material Systems (formerly Textron, US, Figure 2(b)), and Zoltek (US).

2.2.5 Dry-laid materials

Another approach to gas-diffusion-media production, shown to the far right in Figure 3, has been proposed in which PAN fibers (usually in the pre-stabilized form) are dry laid into a thin fiber fleece mat through a carding-combing process. This fleece mat is then bound by hydroentangling, a process in which a curtain of very fine 80–150 μm diameter water jets with spacing of 15–50 jets cm^{-1} is impinged onto the moving mat. This causes some fibers to orient in the through-plane direction and creates a mechanically bonded non-woven fabric. The PAN non-woven mat is then oxidatively stabilized followed by carbonization to 1000–1500 °C. The material can then be optionally filled with carbon or graphite powder and a resin binder followed by carbonization or graphitization to yield a gas-diffusion-media product. Companies currently developing diffusion media based on the dry-laid and hydroentangled non-woven fabric mat include SGL (Germany) and Freudenberg (Germany). Pictures of materials based on this processing sequence are shown in Figure 5(b, c).

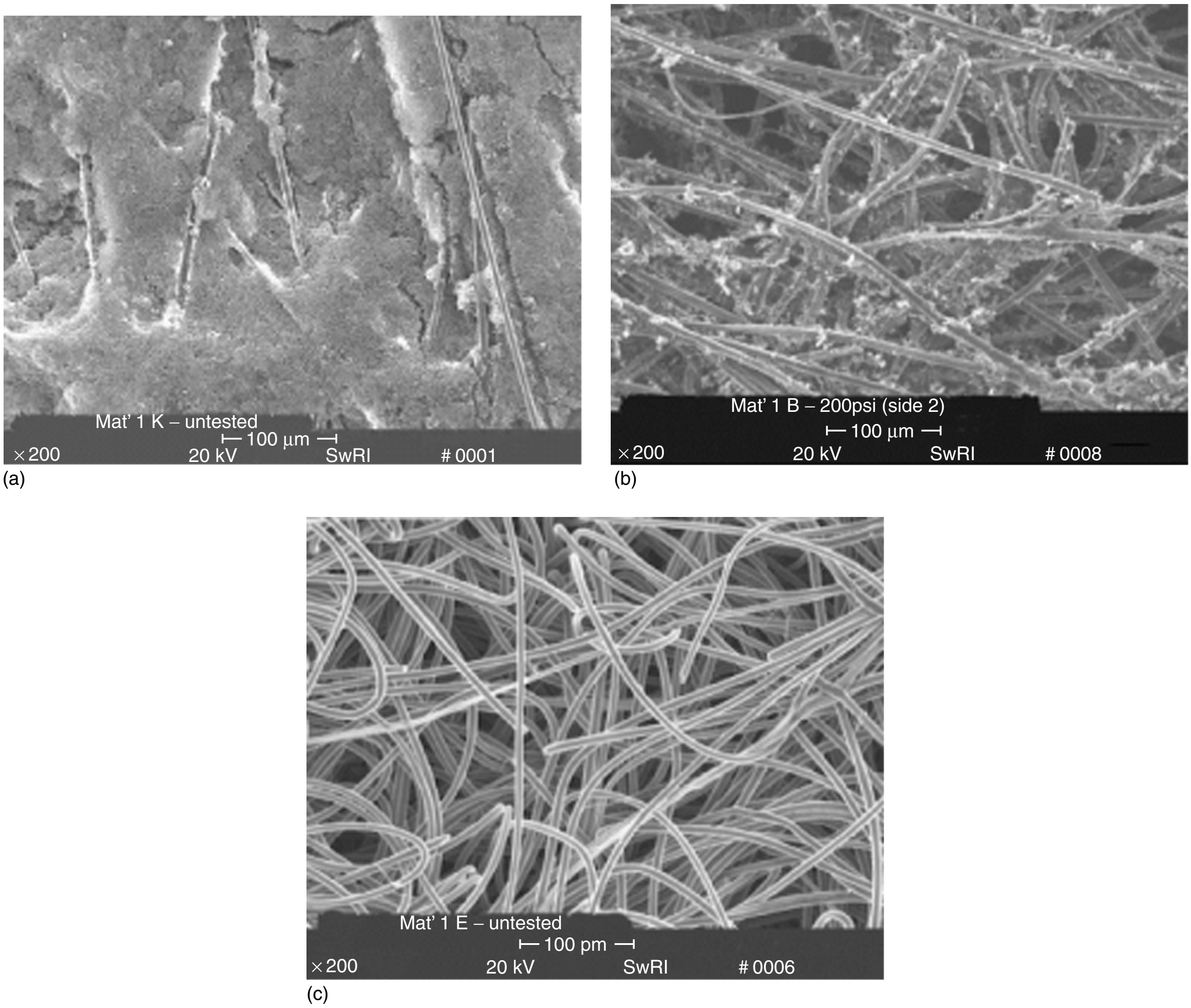

Figure 5. Micrographs (SEM) of (a) wet-laid carbon-filled paper produced by Lydall, (b) dry-laid carbon-filled paper produced by and taken with permission from SGL, (c) dry-laid non-filled paper produced by and taken with permission from Freudenberg. Reference bar indicates 100 µm in each picture.

3 TREATMENTS AND COATINGS

Product water must be transported out of the fuel cell, and the water is present as a liquid under many PEFC conditions. If this water accumulates in a region needed for reactant supply, significant reactant-gas-transport limitations can occur; this phenomenon is often referred to as flooding. Diffusion media are generally made hydrophobic in order to avoid flooding in their bulk. Moreover, the interfaces with adjacent layers are also tailored with coatings or layers to ensure efficient liquid transport into and out of the diffusion layer. This is particularly critical at the cathode catalyst layer interface where inefficient wicking of liquid product water out of the catalyst layer can lead to catalyst layer flooding. Flooding is a poorly understood phenomenon and established diagnostic tools are not yet available to identify in what part of the structure it is occurring. Thus diffusion-media treatment and coating development has been primarily guided by empiricism.

3.1 Bulk treatments

Although carbon substrates used as diffusion media are usually hydrophobic as received from the supplier, they are typically treated with PTFE in order to increase hydrophobicity. This also serves to stabilize this property, since the hydrophobicity of untreated carbon changes due to changes in surface chemistry in an operating cell. Typically, both the cathode and anode diffusion media are PTFE-treated. The need on the cathode side is clear, as most of the product water exits through that layer. However, anode diffusion media are also PTFE-treated. This is important to avoid anode flooding during cell start-up when a warm humid reformate stream may be fed to a cool cell, resulting in significant liquid water condensation.

A wide range of PTFE loadings have been used in PEFC diffusion media, generally falling between 5 and 30 wt% PTFE. The PTFE can be applied to the diffusion media in several ways. Most commonly, the diffusion media is dipped into an aqueous PTFE suspension, excess suspension is allowed to drip off, the remaining solvent is removed by oven drying, and finally the PTFE is heated above 350 °C to sinter the PTFE particles and fix the PTFE to the surface. In dipping, PTFE loading is controlled by adjusting the concentration of the suspension. PTFE can also be applied by many other coating techniques. When attempting to coat one side of the diffusion media, techniques such as spraying and brushing are well suited.

With the dipping application technique, the PTFE distribution through the thickness of the diffusion media is very sensitive to the drying process. Rapid drying in a convective oven tends to result in PTFE concentrated on the exposed surfaces of the diffusion media. In contrast, slow diffusive drying (e.g., air drying) results in PTFE distributed more evenly through the bulk. The effect of drying rate on the PTFE distribution with carbon-fiber paper is illustrated using cross-sectional fluorine maps shown in Figure 6.

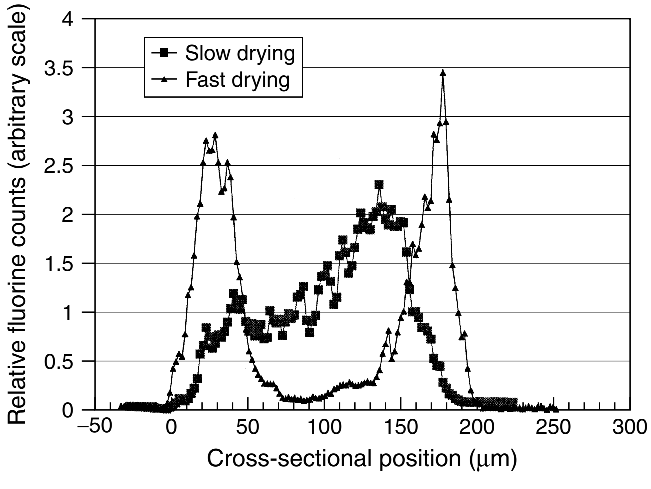

Figure 6. Cross-sectional fluorine maps across carbon-fiber paper (Toray TGP–H–060). PTFE distribution through the paper depends heavily on drying conditions.

3.2 Microporous Layers

In addition to bulk hydrophobic treatments, use of a surface layer or layers is widely practiced. The most common is referred to as a microporous layer, consisting of carbon or graphite particles mixed with a polymeric binder, usually PTFE. Microporous layers have a pore size on the order of the carbon agglomerates, between 100 and 500 nm, as compared with 10–30 μm pore size for carbon-fiber-paper substrates. Their primary purpose is for water management, as they provide effective wicking of liquid water from the cathode catalyst layer into the diffusion media. They also may have utility in reducing electrical contact resistance with the adjacent catalyst layer. The properties of microporous layers can be adjusted by changing the carbon, specifically the particle and agglomerate structure, and the hydrophobicity. Also critical is the nature of the binder; for example a structure has been suggested in which, instead of PTFE, polyvinylidene fluoride (PVDF) is employed.[22]

Techniques developed to apply catalyst pastes to substrates for use in phosphoric acid fuel cells are also applicable to these non-catalyzed pastes. The doctor blade method is common, and others include screen printing, spraying, and rod coating. The carbon paste parameters, such as the solvent choice and solid concentration, must be tailored to provide a coating of desired thickness and substrate penetration with the given application technique. After spreading the paste on the diffusion media, the solvent has to be evaporated slowly to avoid mud cracking. The layer is then heated to remove organics and to sinter the binder. Sometimes the pastes are physically pressed into the substrate, by calendering for example, prior to sintering. Microporous layers are typically less than 50 μm thick.

A commercial example of such a microporous layer is known as Electrode Los Alamos Type (ELAT®) (DeNora North America, Etek Division) which can include carbon-supported catalyst or uncatalyzed carbon. ELAT® layers tailored for PEFCs typically contain uncatalyzed carbon which coats one side of a gas-diffusion substrate, and the coating is positioned against a catalyst-coated membrane. Figure 7 is micrograph of an ELAT® microporous layer coated on a carbon cloth substrate. No underlying visible fibers are visible, and, with the exception of several cracks in the layer, the coating appears smooth on the sub-micron scale.

4 CHARACTERIZATION METHODS

At this early stage in PEFC diffusion-media development, relatively little correlation has been achieved between ex-situ characterization results and in-situ performance. In this section, we describe characterization techniques, some

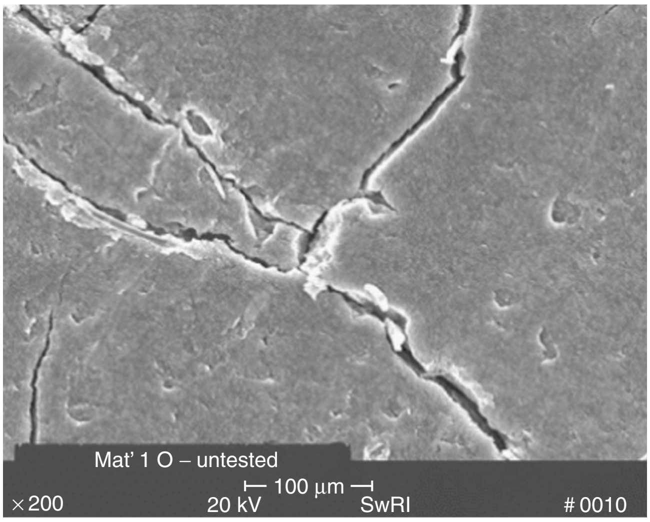

Figure 7. SEM (top view) of ELAT® microporous layer produced by Etek Division of DeNora North America. Coating was applied to carbon-cloth substrate, not visible because it is hidden by the approximately 50 μm thick coating.

established, some under development, that are anticipated to be relevant to fuel cell performance. As the field matures and the methods are honed to focus on parameters critical to PEFC, it is expected that correlations will emerge. Consequently, the requirements of PEFC diffusion media will be able to be increasingly expressed in terms of ex-situ measurements.

4.1 Electrical conductivity

The electrical conductivity of the diffusion media can be successfully correlated with fuel cell performance, especially when using an in-situ measurement that isolates the purely resistive portions of the polarization (e.g., high frequency resistance or current-interrupt). With reference to Figure 1, note that the through-plane direction will be indicated by the z direction, and in-plane properties will be indicated by the x,y directions.

4.1.1 Through-plane conductivity

This property is typically measured by putting a sheet of diffusion media between two flat plates, applying a defined compression, applying a d.c. current through the material, and measuring the plate-to-plate voltage drop. This resistance, sometimes called a through-plane sheet resistance, is most conveniently expressed in units of ohm cm^2. This measured resistance includes contributions from the bulk material and the two contact resistances between diffusion media and plates. In attempts to isolate the bulk resistance, gold plates or even mercury contacts can be used to minimize the contact resistance. However, it is also possible to determine the two resistance contributions, if diffusion media with the same intrinsic bulk properties are available in a variety of thicknesses. In this case, one can extract these values from measurements of the different thickness materials, recognizing that the bulk resistance contribution can be expressed as

$$R_{z,\mathrm{bulk}} = \rho_z d \qquad (1)$$

where ρ_z is the through-plane resistivity (an intrinsic material property with units of ohm cm), and d is the material thickness. The measured resistance in ohms, $R_{z,\mathrm{meas}}$, can be expressed as

$$R_{z,\mathrm{meas}} = \frac{2R_{\mathrm{contact}} + R_{z,\mathrm{bulk}}}{A} \qquad (2)$$

where R_{contact} represents the plate/diffusion-media contact resistance. With the exception of the sample area, A, each of the values in the above two equations depends on the applied compression.

Raw measured resistance data is presented in Figure 8 for carbon-fiber paper of various thicknesses (Toray) as a function of compression pressure between two flat graphite plates. By plotting the data in Figure 8 as resistance vs. thickness with compression pressure as a parameter, one finds R_{contact} for each pressure as the y-intercept. One can then separate the contact and bulk resistance contributions as shown in Figure 9 where results are presented for carbon-fiber paper, with and without 3.5 wt% PTFE. The bulk conductivity results are expressed in terms of a sheet resistance for diffusion media 187 μm thick

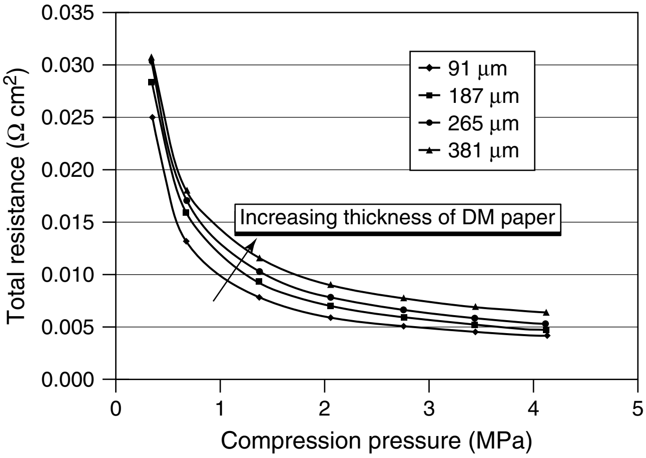

Figure 8. Resistance of carbon-fiber paper (Toray) as a function of uncompressed thickness and compression pressure as measured between two graphite plates.

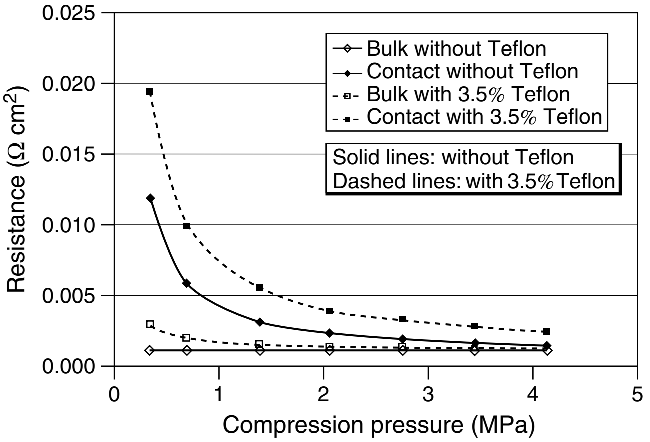

Figure 9. Through-plane resistance of carbon-fiber paper (187 μm uncompressed thickness) and paper/graphite plate contact resistance as a function of compression pressure. The presence of 3.5 wt% PTFE increases the contact resistance to the graphite plates, but has little effect on the bulk resistance.

(uncompressed). The voltage drop due to the bulk resistance of a single sheet is 1.4 mV at 1 A cm^{-2} and depends weakly on the compression at low compression pressures only when PTFE is in the structure. The bulk resistivity, ρ_z, of the PTFE-free structure was found to be 0.073 Ω cm, consistent with the 0.071 Ω cm reported by the supplier using a mercury contact technique. The contact resistance shown in Figure 9 is the major contributor to the total resistance, is a strong function of compression, and is increased if PTFE is in the structure.

The geometry in a fuel cell with channels is more complicated than that of the flat plate ex-situ fixture. The contributions of these ex-situ measured resistances (bulk diffusion-media resistance and plate-to-diffusion-media contact resistance) to fuel cell polarization, $R_{z,\mathrm{FC}}$ would approximately be

$$R_{z,\mathrm{FC}} = \frac{2R_{\mathrm{contact}}}{f_{\mathrm{land}}} + 2R_{z,\mathrm{bulk}} \tag{3}$$

Note that the contact resistance between diffusion media and the catalyst layer is not probed in the ex-situ analysis, and it is not considered here. The contact resistance contribution is inversely proportional to the fraction of active area under compression between lands, f_{land}, and it depends on the local compression pressure on the land. The bulk resistance contribution must be multiplied by two to account for the number of diffusion media, but it is largely independent of the geometry. This is because the in-plane conductivity, at least of conventionally used materials, is sufficient to allow effective utilization of the entire diffusion media bulk, not just material between lands. This is shown in the next section.

4.1.2 In-plane conductivity

This property is typically measured using a four-point probe method. If we imagine a slab of diffusion media of length L_p between the voltage measuring probes, width w, and thickness d, the measured resistance in ohms is

$$R_{xy,\mathrm{meas}} = \frac{\rho_{xy} L_p}{wd} \tag{4}$$

It is convenient to identify the number of square regions present in the measured section, n, as L_p/w. One can then define an in-plane sheet resistance:

$$R_{xy} = \frac{R_{xy,\mathrm{meas}}}{n} = \frac{\rho_{xy}}{d} \tag{5}$$

which has units of ohms (sometimes referred to as ohms square^{-1}). This value represents the in-plane resistance measured across two opposite edges of a square of the material; it is independent of the length of the side of the square but is inversely proportional to the material thickness.

Measurements of this type on carbon-fiber paper (Toray TGP–H–060) yield sheet resistances of 0.26 Ω square^{-1} in one direction (likely the machine direction) and 0.38 Ω square^{-1} in the other (likely the cross-machine direction). This translates to in-plane resistivities of 0.0044–0.0065 Ω cm. Note that the in-plane resistivity of carbon-fiber paper is over an order of magnitude smaller than the through-plane value given above, 0.071 Ω cm. This is due to the alignment of the highly conductive fibers in the plane of the material.

One function of the diffusion media is to conduct electrons to and from the catalyst layer out over the channels, since the catalyst layers themselves have relatively poor electrical conductivity. Using a simple geometric argument illustrated by the schematic in Figure 10, one can estimate the voltage losses associated with this process. (In the following analysis we assume no electrical contact losses between the diffusion media and the catalyst layer over the channel, where there may be very little compressive force. No literature data exists to verify this assumption, and the issue warrants further analysis.) For the following analysis, we consider an arbitrary length of channel, W, running perpendicular to the cross-section shown in Figure 10. For uniform current density, the current carried over the channel is related to the overall current density, i_{tot}, as:

$$I_{\mathrm{channel}} = i_{\mathrm{tot}} C W \tag{6}$$

This current is provided from the adjacent land regions; half of the channel current can be provided from each side. On average, current must be carried in the diffusion media from ¼ of the land width to ¼ of the channel width. The

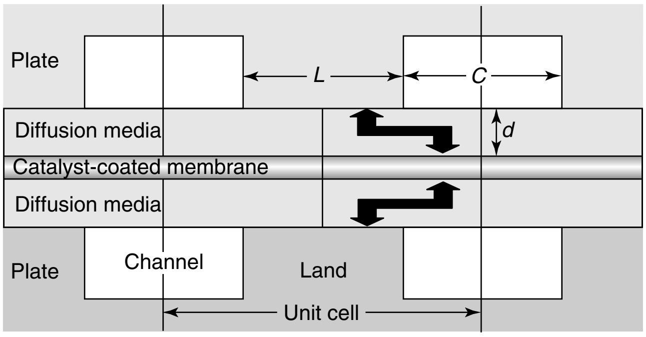

Figure 10. Schematic of cross-section of fuel cell illustrating diffusion media requirement to provide electron conductivity to catalyst regions adjacent to channels.

in-plane resistance to service half of the channel width is therefore:

$$R = \frac{\rho_{xy}}{Wd}\left(\frac{C}{4} + \frac{L}{4}\right) \tag{7}$$

Thus the voltage loss due to this in-plane requirement is

$$\begin{aligned} \Delta V &= \frac{I_{\text{channel}}}{2} R = \frac{\rho_{xy}(C + L)C\ i_{\text{tot}}}{8d} \\ &= \frac{R_{xy}(C + L)C\ i_{\text{tot}}}{8} \end{aligned} \tag{8}$$

If we consider the case where channel width is equal to the land width, this reduces to

$$\Delta V = \frac{R_{xy}C^2\ i_{\text{tot}}}{4} \tag{9}$$

For carbon-fiber paper (Toray TGP–H–060) with R_{xy} of 0.38 Ω square^{-1}, a channel width of 1.5 mm, and an overall current density of 1 A cm^2, the voltage loss is approximately 2 mV. Thus, in this case the in-plane diffusion-media resistance is a small contributor to voltage loss.

The channel/land geometry imposes stricter requirements on the in-plane vs. the through-plane conductivity. To illustrate this, we specify a case in which the in-plane voltage loss is equal to the through-plane bulk loss. Using equations (1) and (7), we arrive at the following resistivity ratio relationship

$$\frac{\rho_{xy}}{\rho_z} = \frac{8d^2}{(C + L)C} \tag{10}$$

For 180 μm thick diffusion media and channel and land widths of 1.5 mm, $\rho_{x,y}/\rho_z$ is equal to 0.06. Using measured values reported above for carbon-fiber paper (Toray TGP–H–060), $\rho_{x,y}/\rho_z$ ranges from 0.06 to 0.09. Thus the electronic conductivity anisotropy of carbon-fiber paper is consistent with the requirement imposed by the PEFC channel/land geometry.

As mentioned in the Introduction, the thermal conductivity of the diffusion media must be sufficient to remove fuel cell waste heat without large temperature gradients. One measurement method involves heating the top surface of the diffusion media with a laser pulse, recording the temperature transient on the opposite diffusion-media surface, and extracting the thermal conductivity from the transient data.[23] However, established measurement methods and reliable data for diffusion-media bulk and interfacial thermal conductivities are not yet available. Work is needed to measure these thermal properties as a function of compression and then to understand their implications for PEFC design and operation.

4.2 Mechanical characterization

In this section, we briefly introduce mechanical properties that are expected to be important for specifying PEFC diffusion media. There is yet very little standardization of methods to measure these properties. Some adoption of standardized methods (e.g., American Society for Testing and Materials (ASTM)) is being attempted, but these methods are geared for other applications and will no doubt be modified for use with PEFC diffusion media.

4.2.1 *Compressive behavior*

To characterize the compressive properties, one places the diffusion media between two flat plates and measures deflection as a function of compressive force. Results for such a measurement are shown in Figure 11(a) for carbon-fiber paper and carbon cloth. In this test, the material was loaded at a rate of 58 kPa s^{-1} up to a load of 2.75 MPa. After reaching the maximum load, the pressure was decreased to zero. This cycle was then repeated 10 times. For both materials, the first compression stroke exhibited a different signal than successive strokes; this reflects a weakening of the material due to its being put under compression for the first time. The cloth is more compressible than the paper; at 2.75 MPa, the paper strain is approximately 24%, whereas the cloth exhibits strain of approximately 52%. One also observes that the materials do not recover to their initial thickness when the load is removed, exhibiting a residual strain. Figure 11(b) shows the residual strain of these materials as a function of cycle number; the paper exhibits better elasticity than the cloth.

4.2.2 *Flexural (or bending) behavior*

In a channel flow field, very compressive materials such as cloths will tend to intrude into the channels and cause

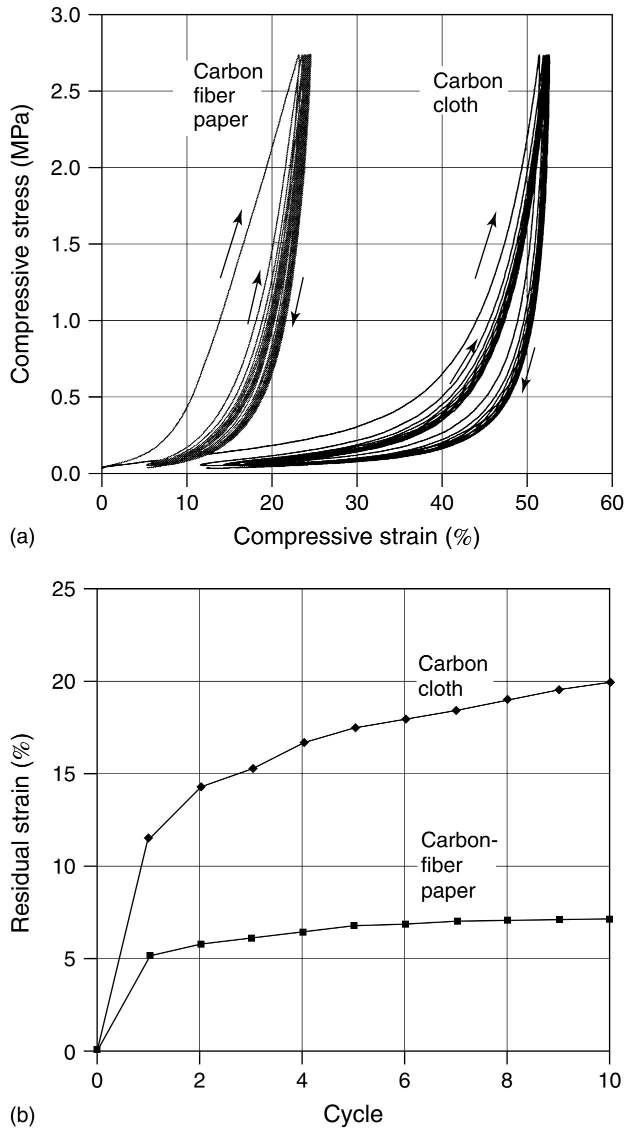

Figure 11. Compression data for carbon-fiber paper (Toray TGP–H–060) and carbon cloth (Textron 1071 HCB). (a) Stress-strain data for 10 cycles loaded at 58 kPa s^{-1} to maximum pressure of 2.75 MPa. (b) Residual strain data as a function of cycle number. Measurements made at Southwest Research Institute (San Antonio, TX, USA).

reactant flow-field pressure drop to increase over that obtained with a carbon-fiber paper, resulting in higher air compressor power requirements. However, the flexibility of the carbon-cloth roll-good product is preferred for manufacturability, suggesting that the flexural strength of the material may need to be optimized in order meet all requirements. There are several reasonable approaches to characterize the flexural behavior of diffusion media. In a method like that described in ASTM D790, a rectangle of diffusion media is supported between two supports and a force is applied in the center. The displacement vs. force response can be used to define a flexural modulus, and the force at break defines a flexural strength. In other approaches, a rectangle of material is clamped at one or both ends. The material is then moved so as to bend it, and the modulus and strength is determined by the response. Examples of these techniques are the Taber test (material clamped at both ends, ASTM D5650) and a cantilever beam test (ASTM D747). These methods are not relevant to a material with an extremely low flexural modulus, such as carbon cloth.

4.3 Thickness, porosity, and pore size distribution

The porosity can be calculated from measuring the bulk density of diffusion-media material, which is calculated from the areal weight and the thickness. Because the material thickness can depend heavily on the compressive force, gauges are required that exert a small but defined pressure on the sample under test. The pressure used should be reported when reporting the thickness. The size of the gauge foot and the length of time under compression before measurement is taken should also be controlled for consistent results.

Using the thickness and the areal weight, one can calculate the bulk density, ρ_{bulk}. The average porosity of diffusion media can be estimated simply using the bulk density of the material and the real density of the solid phase, ρ_{real}. This value can be measured by a gas pycnometer; it varies between 1.6 and 1.9 g cm^{-3} for carbon-based gas-diffusion media. The porosity, ε, also depends on the compressed thickness of the diffusion media under load, d, relative to the uncompressed value d_o.

$$\varepsilon = 1 - \left(\frac{\rho_{\text{bulk,o}}}{\rho_{\text{real}}}\right)\left(\frac{d_o}{d}\right) \tag{11}$$

where $\rho_{\text{bulk,o}}$ is the bulk density of the diffusion media when uncompressed.

The pore size distribution in diffusion media is difficult to characterize because the material comprises an interconnected porous network rather than a set of discrete pores. Nevertheless, there is a need to characterize this network to provide parameters for transport models and because it is important for material design. Because the porous network is irregular, different methods can yield different pore size distributions for the same material, as illustrated below.

Mercury porosimetry is a well-known method that can be applied to diffusion media. In this method, mercury with its very high surface tension is forced into the pores of the samples. The amount of mercury uptake as a function of pressure allows one to calculate a pore

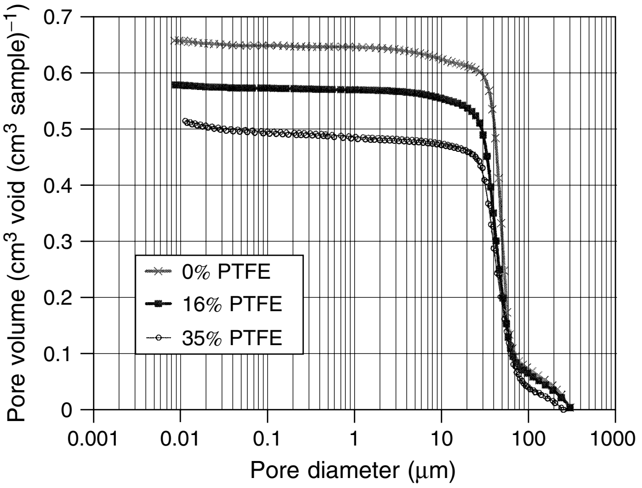

Figure 12. Mercury porosimetry results for uncompressed carbon-fiber paper (Toray TGP–H–060) loaded with different amounts of PTFE. Large majority of void volume is present in pores with diameter registering greater than 10 μm.

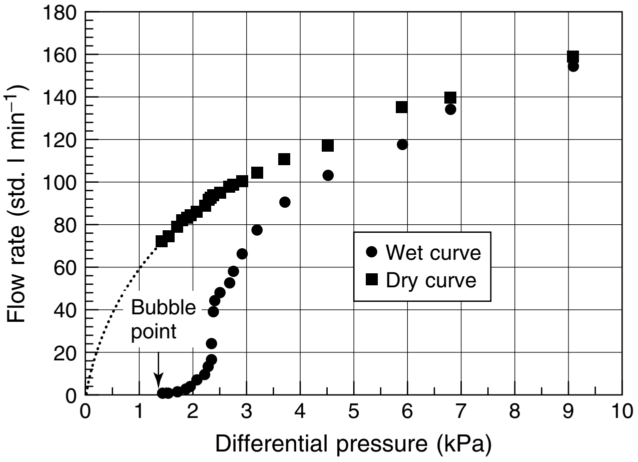

Figure 13. Flow vs. pressure results for capillary-flow experiment on carbon-fiber paper (Toray TGP–H–060, 0 wt% PTFE) with Silwick as wetting agent. Bubble point is associated with breakthrough at 1.4 kPa.

size distribution. From the total uptake of mercury at the maximum applied pressure, the porosity can be calculated. Figure 12 shows the pore size distribution of carbon-fiber paper with different PTFE content, showing as expected that the pore volume of the material decreases with increased PTFE loading. Over 90% of the pore volume resides in pores with diameter of 10 μm or higher. The average pore diameter as measured by mercury porosimetry is observed to be between 30–40 μm for the carbon-fiber paper samples represented in Figure 12. This defines a volume-based mean pore size; 50% of the pore volume is located in pores with diameter larger than this size, and 50% is located in pores smaller than this size.

In another method, capillary flow porometry, the diffusion media is brought into contact with a low-surface-tension liquid that wicks into the sample. One example of such a solution is a silicone oil called Silwick. By applying a gas pressure across the flooded sample, the liquid can be forced out of the pores. The pressure at which gas begins to flow due to clearing of the first pore is called the bubble point, and this point can be used to calculate the maximum pore size. The pressure is then further increased and progressively smaller pores are cleared until the sample is fully dried. The details of the theory and the measurement method can be found elsewhere.[24]

Raw flow vs. pressure drop data from a through-plane capillary-flow-porometry experiment with carbon-fiber paper is shown in Figure 13. The bubble point is reflected by the onset of flow occurring at about 1.4 kPa; the wet curve was then traced as the sample was being cleared of liquid. The bubble point corresponds to a pore diameter of 46 μm. A dry curve was also taken in a subsequent scan. From the difference between the dry and the wet curve, one can calculate the pore size distribution. The pore size distribution determined from the data in Figure 13 is shown in Figure 14 where the cumulative flow is plotted against pore size. The average pore size as measured by capillary-flow porometry, 23 μm in this case, defines a flow-based mean pore size: 50% of the flow through the sample flows through larger diameter pores, and 50% flows through pores smaller than this size. By design of a sample holder that passes flow in the plane of an annular sample, the in-plane flow-based pore size distribution can also be determined. For the Toray TGP–H–060 material, the average pore diameter was typically within 5 μm of the through-plane result.

Results for average (mean-volume and mean-flow) and maximum (bubble point) pore diameters are shown in

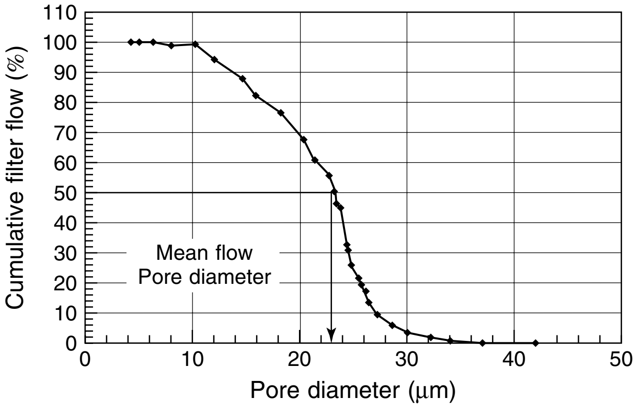

Figure 14. Cumulative-filter-flow pore size distribution from capillary-flow results shown in Figure 13. Mean-flow pore diameter for carbon-fiber paper (Toray TGP–H–060) is 23 μm.

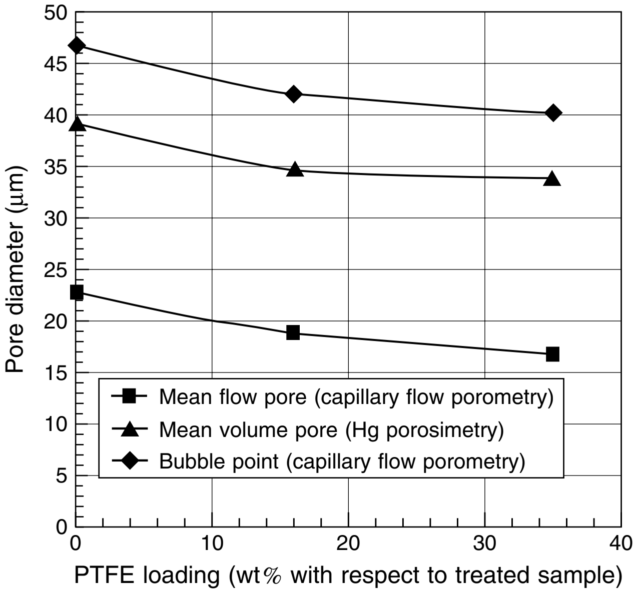

Figure 15. Various measures of pore diameter for carbon-fiber paper (Toray TGP–H–060) as a function of PTFE loading. Each method is sensitive to a different feature of the irregular porous structure and thus yields different results.

Figure 15 for Toray TGP–H–060 with various amounts of PTFE. For all measures of pore characterization, the average diameter decreases with increasing PTFE content. The volume-based average pore size is significantly greater than the flow-based pore size. To understand this, we consider that a single gas molecule flowing through these materials would experience openings of various sizes as it passed through the material, because of the irregular pore structure. The capillary method identifies the minimum restriction observed during a pass through the material. Mercury porosimetry, on the other hand, reveals porosity as soon as the mercury penetrates the porous structure, and the large openings in contact with the material surface are recorded as large-diameter pores. These large pores do not pass all the way through the material, but in mercury porosimetry they are identified as large pores nonetheless.

4.4 Fluid permeability

In this section, we introduce several methods that can be used to characterize gas and liquid permeability through diffusion media.

4.4.1 Gas transport

There are different models of gas transport in porous media, which are based on various conceptualizations of the porous network. One example is the Dusty Gas Model in which the porous network is represented by large dust particles uniformly distributed in space and the movement of gas molecules is described by the kinetic theory of gases.[25, 26] Another formulation is called the Mean Transport Pore Model (MTPM) in which the gas transport is assumed to occur in cylindrical pores with a distribution of radii. With the MTPM, parameters characterizing the network are the mean pore radius $\langle r \rangle$, the squared transport pore radius $\langle r^2 \rangle$ (which reflects the pore size distribution), and ψ, the ratio of the porosity to the tortuosity.[27, 28] Estimates of material properties and transport parameters must be obtained by performing diffusion and convection experiments, but the specific parameters extracted from the data depend on the model being employed.[29, 30]

To measure diffusion coefficients, the transport of a gas across the porous media is typically monitored (e.g., using a gas chromatograph (GC)) with no pressure drop across the sample. Generally, effective diffusion coefficients are used; these include effects of material porosity and tortuosity. Diffusion coefficients in PEFC gas-diffusion media in most cases reflect bulk as opposed to Knudsen diffusion because the diffusion-media pore diameters (10s of micrometers) are much larger than the mean free path of the gas molecules (approximately 100 nm). Knudsen diffusion may influence transport in microporous layers where the pore sizes can approach the mean free path.

Convective-flow resistance is typically characterized by the Darcy coefficient that can be estimated by applying a pressure drop and observing the flow. Many diffusion-media developers characterize the resistance to convective gas flow in the through-plane direction, and a variety of methods are employed. All of them involve defining a gas flow rate through a given sample area at a given pressure drop. For low flow materials such as those with a microporous layer, one sometimes expresses this parameter as the time required to pass a certain volume of flow through a given sample at a given pressure drop (e.g., the Gurley parameter). A more fundamental way to characterize this property is to report the Darcy coefficient, which relates the convective driven flux to the pressure drop via Darcy's law:

$$V = k_{\mathrm{d}} \frac{a}{\mu l} \Delta P \qquad (12)$$

where V is the volumetric flow rate, k_{d} is the Darcy coefficient ($1\,\mathrm{Darcy} = 10^{-12}\,\mathrm{m}^2$), a is the cross-sectional area through which the flow passes, μ is the gas viscosity, l is the length of the convective path, and ΔP is the pressure differential across the sample. We have measured the through-plane Darcy coefficient of uncompressed Toray TGP–H–060 carbon-fiber paper to be approximately

5–10 Darcy's. Although this property can be easily measured, no success has been reported at correlating through-plane convective-flow resistance with fuel cell performance. This is not surprising since the primary transport mode in the through-plane direction in diffusion media is typically diffusion and not convection.

A more relevant parameter for fuel cell use is the Darcy coefficient of the diffusion media in the in-plane direction. This is relevant for interdigitated flow fields as well as for understanding flow between channels over lands in the case of serpentine flow fields. The Darcy coefficient can be estimated using a two-channel cell in which gas is driven into the plane of the diffusion media from one channel to an adjacent channel. For Toray TGP–H–060 carbon-fiber paper, compressed to approximately 75% of initial thickness, we have determined a coefficient of approximately 5–10 Darcy's, the same range as the through-plane values.

4.4.2 Liquid transport

Whereas capillary-driven liquid flow through diffusion media (discussed below) may predominate in fuel cell operation, convective liquid transport may also be important. A liquid permeability test can be used to characterize the resistance to liquid flow through a sample. In this method, a column of liquid is put on top of the porous medium, and a pressure is applied to force the liquid through. If convective transport of water is important in fuel cell operation, then one might expect results from such a method to correlate with diffusion-media flooding tendency.

Figure 16 shows flow rate vs. pressure drop results from a series of measurements in which either silicone oil or water were flowed through 1 mm thick carbon-fiber paper with various levels of PTFE. The hydrohead pressure, indicated by the x-intercept, represents the pressure needed to first get the liquid into the material. The curves for the silicone oil, a low surface tension liquid that is wetting with respect to the diffusion media, go approximately through the origin, showing that no hydrohead pressure was needed to initiate liquid flow. At a given pressure drop, the flow rate decreases with a higher PTFE loading due to the decrease in porosity.

The results with water exhibit a larger slope reflecting the smaller viscosity relative to silicone oil. The high PTFE loaded sample reveals a hydrohead pressure of 1.5 kPa. Data involving a non-wetting liquid such as water are difficult to reproduce, as they are history-dependent. A dry sample shows highest resistance but the pressure decreases when the test is repeated with the same sample. After 5–15 tests, depending on the sample, the pressure reaches a constant value once the amount of water remaining within the sample has reached a steady state.

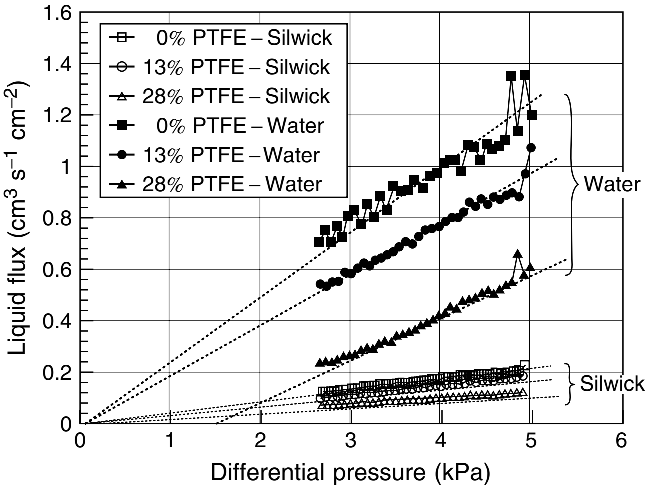

Figure 16. Liquid permeability results for carbon-fiber paper (Toray TGP–H–1.0T, 1 mm thick) as a function of PTFE loading. Results are shown for Silwick and water. The result with water and high PTFE loading indicates a hydrohead pressure of 1.5 kPa.

Note in Figure 16 that the flux of water at 1 A cm^{-2} is only 1×10^{-4} cm^3 s^{-1}cm^{-2} as compared with fluxes shown in Figure 16 that are up to four orders of magnitude larger. The relevance of the results of this test method to fuel cell operation thus remains to be established.

4.5 Surface energy and contact angle

The hydrophobic properties of diffusion media are often adjusted to tailor their interaction with liquid water, either by bulk treatment or by addition of layers on one or both surfaces. In this section, we discuss methods of characterizing the interaction between liquid water and the diffusion media.

Surface energy defines the work required to enlarge the surface area of matter.

$$\sigma = \left(\frac{\partial G}{\partial A}\right)_{n,P,T,V} \tag{13}$$

The correlation between surface energy and the contact angle is given by Young's equation

$$\sigma_s = \sigma_{l,s} + \sigma_l \cos \Theta \tag{14}$$

where σ_s is surface energy of the solid face, σ_l is surface energy of the liquid face (equivalent to surface tension), $\sigma_{l,s}$ is surface energy of the liquid-solid interface, and Θ is contact angle of the liquid on the surface. A liquid completely wets a solid surface when the contact angle is 0° and can be considered resistant to wetting when the contact angle is greater than 90°. In general, a liquid will wet a surface when the surface energy of the solid is larger than the surface energy of the liquid.[31]

4.5.1 Measuring contact angles of diffusion media

When the liquid is resistant to wetting (contact angle greater than 90°), there are several techniques that can safely be applied.

Sessile drop method

The most common method for measuring contact angle on a diffusion-media surface is called the sessile drop method. In this technique, a droplet of water is set on the surface and the contact angle is measured by fitting a tangent to the three-phase point where the liquid surface touches the solid surface. This can be done either by digitizing the image of the drop and using a computer program, or by using a microscope with angle measuring capability. The drop size used is small, no more than approximately 1 mm, so as not to influence the contact angle due to weight of the drop itself. Also, data must be taken before significant evaporation occurs. Using this method, we have measured contact angles of water on carbon-fiber paper (Toray TGP–H–060) of 135°, 156°, and 164° for papers treated with 0, 9 and 23 wt% PTFE, respectively.

Wilhelmy methods

In this technique, a rectangular-shaped piece of diffusion media is dipped vertically into water and the weight of the diffusion media is measured with a sensitive balance. In a static version of this method, the sample is inserted a known distance and the force is measured. The force includes contributions from the sample weight, the repelling or attracting force caused by the water-to-solid interaction, and the buoyancy force. The sample weight is known, and the buoyancy force can be calculated. These values are subtracted from the measured force, and the contact angle can be calculated from the remaining force using

$$F = L_{1,s}\sigma_1 \cos\Theta \tag{15}$$

where F is the remaining force, and $L_{1,s}$ is the length of the liquid–solid interface. For a sample in the form of a rectangular strip, the typical sample configuration, $L_{1,s}$ is equal two times the sum of the paper width and thickness. The Wilhelmy method requires that both surfaces of the diffusion media have identical wetting characteristics. Thus, when diffusion media with two different surfaces are tested (such as when a microporous layer is applied to one side) two samples must be attached together with double-sided tape so that the surfaces of interest are on the outside.

The drop-shape on rough surfaces, like those of diffusion-media substrates, depends on the surface texture. For this reason, the Wilhelmy plate method gives more reliable results than the sessile drop measurement because a larger three-phase boundary is probed.

Further improvements in accuracy can be attained by using a dynamic Wilhelmy method. The arrangement is similar to that of the static method, but the diffusion media is moved at a constant rate into the solution as the force is monitored. At a predetermined depth, the movement is reversed and the sample is removed at the same rate. This method leads to a larger number of observations at different spots along the moving three-phase line and thus allows for better statistics than the static Wilhelmy approach. Rather than generating a single average contact angle, this method provides two separate characteristics of the wetting properties: an *advancing angle* (from the sample insertion phase) and a *receding angle* (from the sample removal phase). The advancing angle reflects the surface attraction for the liquid, and the receding angle reflects the surface repellency of the liquid. The receding angle is important information to predict the behavior of liquid water on the channel side of the diffusion media.

Figure 17 shows results from 4 wt% PTFE treated carbon-fiber paper in the dynamic Wilhelmy test. After attaching the sample and taring the balance, the sample was inserted at a rate of 8.5 mm min^{-1} to a depth of 15 mm. It was then held there for 30 s before being withdrawn. The results from the first 3 mm of immersion depth reflect establishment of the meniscus. The straight-line section between

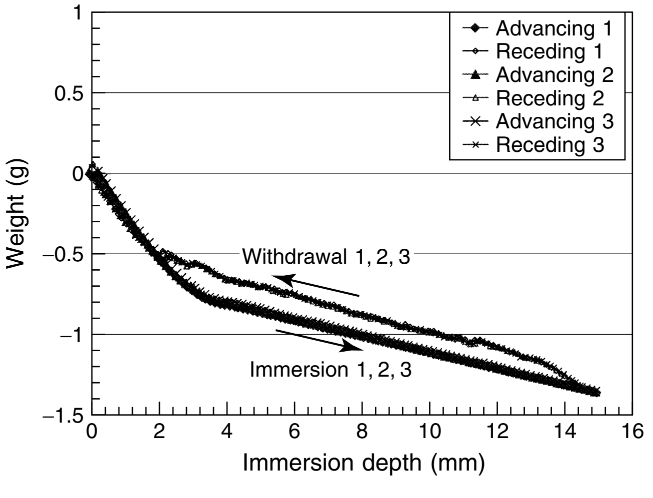

Figure 17. Dynamic Wilhelmy result for carbon-fiber paper treated with 4 wt% PTFE. Results were independent of cycle indicating that paper internals were not wetted.

3 and 15 mm is used to extract the advancing contact angle. This is done by extrapolating back to zero immersion depth to eliminate the buoyancy force. The intercept is the force due to the water-solid interaction, and the advancing contact angle can be calculated using equation (15). A similar procedure is applied to the straight-line section from sample withdrawal. For this sample, advancing and receding angles were found to be 170° and 134°, respectively. The data from a second insertion and withdrawal overlap those from the first, showing no sample wetting occurred and lending credibility to the results. The average of the advancing and receding angle, 152° is reasonably consistent with the sessile drop results for this sample of 140–150°.

Figure 18 shows the dynamic Wilhelmy result with untreated carbon fiber paper. From these data, angles of 154° (advancing) and 13° (receding) are determined from the first insertion and withdrawal. However, the second insertion shows forces much higher than those of the first; this result is due to the diffusion media becoming hydrophobic during the first insertion-hold-withdrawal cycle because of residual liquid water fillings on the surface. Non-overlapping immersion curves as illustrated in Figure 18 can also be due to water filling of the internal diffusion-media pores during the first wetting-dewetting cycle. To understand cases in which water penetrates into the porous material, one would need to characterize the contact angle associated with internal diffusion media surfaces. Suitable methods to characterize the wetting (or wicking) properties of internal diffusion-media surfaces are not yet well-established and data are not yet available. Thus method development is needed, as are efforts to correlate diffusion-media wetting properties with fuel cell performance.

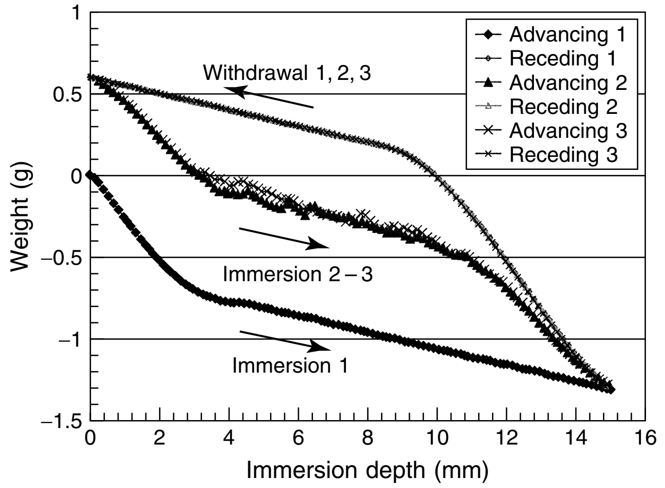

Figure 18. Dynamic Wilhelmy result for three immersions-withdrawals of carbon-fiber paper (Toray TGP–H–060) in water. First immersion yields different results from subsequent immersions due to wetting of paper internals.

4.5.2 Determining surface energy from contact angle data

The surface energy of diffusion media surfaces can be estimated using an approach suggested by Zisman.[32] In this approach, contact angles are needed on the solid surface of interest for two or more liquids with substantially different surface tensions. One then constructs a Zisman plot: the liquid surface energy vs. $\cos\Theta$. The surface energy of the solid phase is defined where a line through the data crosses $\cos\Theta = 1$. The method is based upon the theory that the interaction parameter ($\sigma_{s,l}$) is zero when the surface energy of the liquid is equal to the surface energy of the solid. This simplification is a first approximation; for more precision, one can estimate $\sigma_{s,l}$ from the surface energies of the pure solid and the pure liquid using more sophisticated theory.[33–35]

4.6 Fuel cell characterization

Diffusion-media development still relies heavily on in-situ testing, because well-established correlations between in-situ performance results and ex-situ characterization data are not yet available. As described above, diffusion media should ideally operate well under a variety of humidification conditions. Single cell testing can be used to screen diffusion-media candidates and determine if they provide good performance and robust operation.

One such single-cell screening test is illustrated by the results shown in Figure 19. Data were taken using single fuel cells with 50 cm^2 active area. The cell was operated under the following conditions: 80 °C, 150 kPa absolute pressure, 100% H_2 feed to anode at 2.0 stoichiometry, air feed to the cathode with 2.0 oxygen stoichiometry. The cell was held at 0.6 V, and the current and high-frequency (1 kHz) resistance were monitored. The relative humidity of the anode and the cathode were maintained equal to one another, and steady-state data were taken at seven different humidification conditions.

The figure shows the response of current and high frequency resistance to changes in the relative humidity of the inlet streams for two different cells using different versions of carbon-fiber paper (Toray TGP–H–090) on the cathode. In one case the paper was treated with approximately 4 wt% PTFE and in the other it was used as received. For the anode diffusion media, Toray TGP–H–060 with 7 wt% PTFE was used in both cells. With excessive humidification, the current dropped due to flooding in both cases, but much more so when using the untreated paper. At low humidification, the current dropped due to drying of the

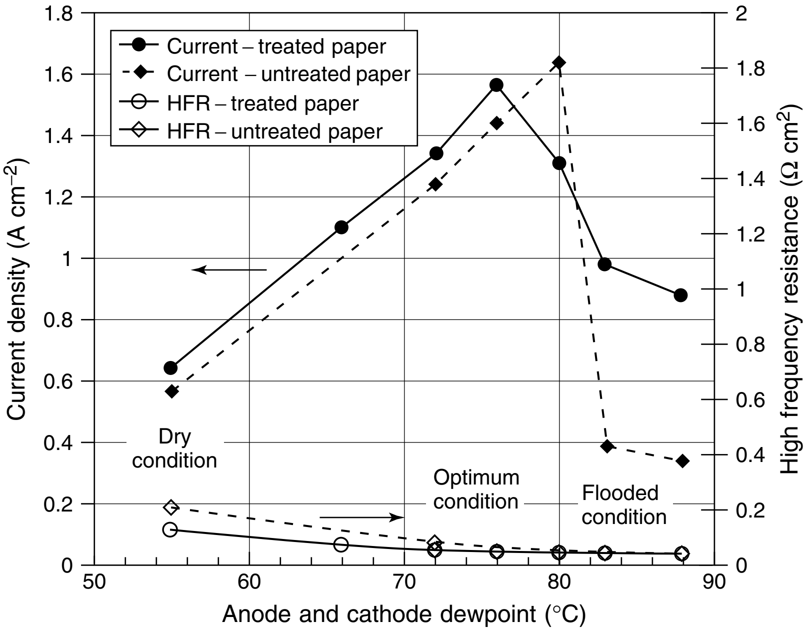

Figure 19. Current and high-frequency resistance data from two single-cell fuel cells (treated vs. untreated cathode diffusion media) as a function of cathode and anode dewpoint (maintained equal). Conditions: constant voltage at 0.6 V, 50 cm^2 active area, 80 °C, 150 kPa absolute, 100% H_2 feed at 2.0 stoichiometry, air feed at 2.0 oxygen stoichiometry.

membrane for both diffusion media, slightly more so for the untreated paper. Membrane drying is indicated by the increase in high-frequency resistance in this region. Optimum operation for this particular fuel cell occurs at a high frequency resistance of 0.06–0.07 Ω cm^2. An ideal diffusion media would resist flooding and membrane and catalyst layer drying, thus maximizing the peak current and the humidification range over which the current remained high. Figure 20 shows polarization data for the two cells represented in Figure 19. The treated paper shows much better resistance to flooding in the high current density region relative to the untreated version, consistent with the results in the flooding region shown in Figure 19.

Multiple cell (or short stack) testing of 10–30 cells has proven to be useful for comparing different types of catalyst coated membranes in the same stack (see **Beginning-of-life MEA performance — Efficiency loss contributions**, Volume 3). This same approach can generally not be applied when testing different diffusion-media candidates. For a fair comparison, the cells must have the same resistance to flow in order to maintain equal reactant stoichiometry from cell to cell. Thus, diffusion media in a stack must have very similar flow resistance, compression properties, and water management. Although short stack testing is not suited for comparing different substrates, it can prove useful for examining effects of relatively small adjustments of microporous layer or treatment parameters.

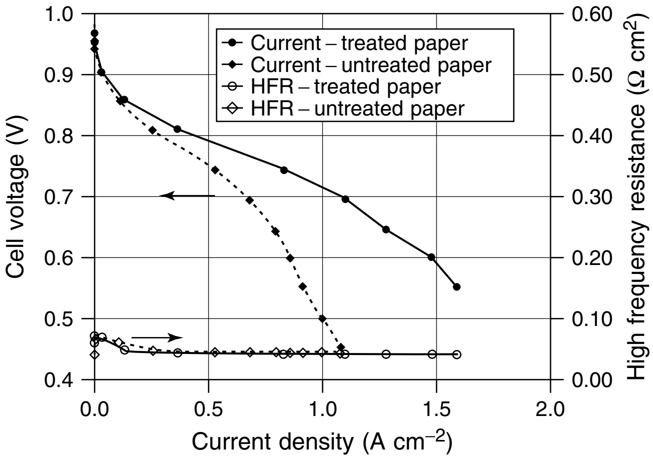

Figure 20. Polarization curve and high-frequency resistance from two single-cell fuel cells (treated vs. untreated cathode diffusion media). Conditions: 50 cm^2 active area, 80 °C, 270 kPa absolute, 2.0/2.0 stoichiometry on 100% H_2/air down to 0.2 A cm^2 (constant flow below), 100%/50% relative humidity on anode/cathode.

XREF

5 CONCLUSIONS

PEFC gas-diffusion media has perhaps been the component most dependent on empiricism for its development. Despite its many functions, it has received very little development attention, as evidenced by the scarcity of publications on PEFC diffusion media in the literature. However, currently available diffusion media do not meet long-term requirements for cost, and development of less expensive materials is needed. Additionally, issues of flooding under steady-state and transient (e.g., start-up) conditions as well as low-current stability issues demand careful diffusion-media design. Moreover, it is likely that durability is significantly impacted by diffusion-media substrate and treatment in ways that are not yet understood.

As illustrated in this chapter, there are many candidate materials and process variables that can be adjusted to develop optimum materials for a given application. In support of this, much remains to be done in terms of establishing characterization methods and property-performance relationships. The diffusion media will need to receive much more focussed attention to development before the widespread commercialization of PEFC fuel cells becomes a reality.

ACKNOWLEDGEMENTS

This work draws in part on characterization method developments made by Mike Schoeneweiss (physical properties), Wenbin Gu (electrical properties), and David Wood (physical and permeability properties). Rick Waldo and Curtis Wong provided analytical support.

LIST OF SYMBOLS

a	cross-sectional area of flow (cm^2)
A	area of sample (cm^2)
C	channel width (cm)
d	thickness of diffusion media (cm)
F	force on balance (g)
G	Gibbs free energy (J)
f_{land}	fraction of active area under compression between lands
k_{d}	Darcy coefficient (1 Darcy = $10^{-12}\,\mathrm{m}^2$)
I_{channel}	current carried over channel section (A)
i_{tot}	current density ($\mathrm{A\,cm}^2$)
l	convective flow length (cm)
L	land width (cm)
$L_{\mathrm{l,s}}$	length of liquid–solid interface in Wilhelmy experiment (cm)
L_{P}	distance between voltage sense probes in 4-point measurement (cm)
n	number of squares in in-plane measurement
R	in-plane resistance of diffusion media carrying current between land/channel (Ω)
R_{contact}	contact resistance between diffusion media and bipolar plate ($\Omega\ \mathrm{cm}^2$)
R_{xy}	sheet resistance, in-plane (Ω or Ω per square)
$R_{xy,\mathrm{meas}}$	measured resistance, in-plane Ω)
R_z	sheet resistance, through-plane ($\Omega\,\mathrm{cm}^2$)
$R_{z,\mathrm{bulk}}$	sheet resistance of bulk, through-plane ($\Omega\,\mathrm{cm}^2$)
$R_{z,\mathrm{FC}}$	sheet resistance in actual fuel cell environment, through-plane ($\Omega\,\mathrm{cm}^2$)
$R_{z,\mathrm{meas}}$	measured resistance, through-plane (Ω)
V	volumetric flow rate ($\mathrm{cm}^3\,\mathrm{s}^{-1}$)
w	sample width in 4-point measurement (cm)
W	length of the arbitrary segment of channel
ΔP	pressure drop (Pa)
ΔV	voltage loss due to in-plane diffusion media resistance (V)
ε	diffusion media porosity
μ	viscosity (Pa s)
Θ	contact angle (degrees)
ρ_{bulk}	bulk density of diffusion media ($\mathrm{g\,cm}^3$)
ρ_{real}	density of solid portion of diffusion media ($\mathrm{g\,cm}^3$)
ρ_{xy}	resistivity, in-plane (Ω cm)
ρ_z	resistivity, through-plane (Ω cm)
ρ_{l}	surface energy (equivalent to surface tension) of liquid ($\mathrm{N\,m}^{-1}$)
$\rho_{\mathrm{l,s}}$	surface energy of liquid–solid interface ($\mathrm{N\,m}^{-1}$)
ρ_{s}	surface energy of solid ($\mathrm{N\,m}^{-1}$)

Subscripts

o	uncompressed
xy	in-plane of diffusion media
z	perpendicular to plane (through-plane) of diffusion media

REFERENCES

1. W. He, J. S. Yi and T. V. Nguyen, *AIChE J.*, **46**, 2053 (2000).
2. D. R. Baker and R. M. Darling, *Int. J. Transport Phenomena*, **3**, 231 (2001).
3. G. Faita and C. Mantegazza, 'US 5,482,792: Electrochemical Cell Provided with Ion Exchange Membranes and Bipolar Metal Plates', Patent issued Jan. 9 (1996).
4. M. S. Wilson and C. Zawodzinski, 'US 6,207,310: Fuel Cell with Metal Screen Flow Field', Patent issued Mar. 27 (2001).
5. E. A. Ticianelli, *J. Electroanal. Chem.*, **387**, 1 (1995).
6. D. S. Chan and C. C. Wan, *J. Power Sources*, **50**, 261 (1994).
7. K. Miwa, K. Shimazu and H. Fukui, 'US 4,851,304: Electrode Substrate for Fuel Cell and Process for Producing the Same', Patent issued Jul. 25 (1989).

8. R. Lindstrom, 'US 4,647,359: Electrolytic Gas Diffusion Electrode Employing Thin Carbon Cloth Layer', Patent issued Mar. 3 (1987).
9. A. Koschany, C. Lucas and T. Schwesinger, 'US 5,998,057: Gas Diffusion Electrode for Polymer Electrolyte Membrane Fuel Cells', Patent issued Dec. 7 (1999).
10. S. A. Campbell, J. Stumper, D. P. Wilkinson and M. T. Davis, 'US 6,060,190: Electrochemical Fuel Cell Membrane Electrode Assembly with Porous Electrode Substrate', Patent issued May 9 (2000).
11. Y. Sugawara, M. Uchida, H. Ohara, Y. Fukuoka and N. Eda, 'US 6,194,094: Polymer Electrolyte Fuel Cell', Patent issued Feb. 27 (2001).
12. R. R. Fredley, 'US 5,998,058: Porous Support Layer for an Electrochemical Cell', Patent issued Dec. 7 (1999).
13. R. J. Allen, R. Lindstrom and W. Juda, 'US 4,293,396: Thin Carbon-Cloth Based Electrolytic Gas Diffusion Electrodes, and Electrochemical Cells Comprising the Same', Patent issued Oct. 6 (1981).
14. M. DeMarinis, E. S. De Castro, R. J. Allen and K. Shaikh 'US 6,103,077: Structures and Methods of Manufacture for Gas Diffusion Electrodes and Electrode Components', Patent issued Aug. 15 (2000).
15. G. A. Eisman, W. B. Maynard, R. H. Farkash and C. M. Carlstrom, 'Combined Fuel Cell Flow Plate and Gas Diffusion Layer', Patent issued Aug. 28 (2001).
16. M. S. Wilson, 'US 5,952,119: Fuel Cell Membrane Humidification', Patent issued Sep. 14 (1999).
17. T. R. Ralph, G. A. Hards, J. E. Keating, S. A. Campbell, D. P. Wilkinson, M. Davis, J. St-Pierre and M. C. Johnson, *J. Electrochem. Soc.*, **144**, 3845 (1997).
18. L. R. Jordan, A. K. Shukla, T. Behrsing, N. R. Avery, B. C. Muddle and M. Forsyth, *J. Power Sources*, **86**, 250 (2000).
19. T. Zawodzinski, J. Bauman, F. Uribe, S. Gottesfeld, E. S. DeCastro and M. DeMarinis, 'Carbon Cloth Gas Diffusion Backings for High Performance PEFC Cathodes', in 'Proceedings of the Second International Symposium on Proton Conducting Membrane Fuel Cells', S. Gottesfeld and T. F. Fuller (Eds), Electrochemical Society, Pennington, NJ, PV98-27 pp. 1–9 (1999).
20. W. Lee, C. Ho, J. W. Van Zee and M. Murthy, *J. Power Sources*, **85**, 45 (1999).
21. C. Segal, 'Carbon Fiber Markets' presented at Carbon Fiber Conference-2001 sponsored by Intertech, Bordeaux, France, October (2001).
22. I. Cabasso, Y. Yuan and X. Xu, 'US 5,783,325: Gas Diffusion Electrodes Based on Poly(Vinylidene Fluoride) Carbon Blends', Patent issued July 21 (1998).
23. R. J. Parker, R. J. Jenkins, C. P Butler and G. L. Abbott, *J. Appl. Phys.*, **32**, 1679 (1961).
24. A. K. Jena and K. M. Gupta, *J. Power Sources*, **80**, 46, (1999).
25. R. Jackson, 'Transport in Porous Catalysts', Elsevier, Amsterdam (1977).
26. E. A. Mason and A. P. Malinauskas, 'Gas Transport in Porous Media: The Dusty Gas Model', Elsevier, Amsterdam (1983).
27. D. Arnošt and P. Schneider, *Chem. Eng. J.*, **57**, 91 (1995).
28. P. Schneider, *Chem. Eng. Sci.*, **33**, 1311 (1978).
29. J. Valuš and P. Schneider, *Appl. Catal.*, **1**, 355 (1981).
30. P. Fott and G. Petrini, *Appl. Catal.*, **2**, 367 (1982).
31. R. J. Good and L. A. Girifalco, *J. Phys. Chem.*, **64**, 561 (1960).
32. W. A. Zisman, *ACS Adv. Chem. Ser.*, **43**, 1–51 (1964).
33. R. J. Good and L. A. Girifalco, *J. Appl. Polym. Sci.*, **64**, 561 (1960).
34. R. M. Fowkes, *Ind. Eng. Chem.*, **56**, 12 (1964).
35. D. K. Owens and R. C. Wendt, *J. Appl. Polym. Sci.*, **13**, 1741 (1969).